ISEF 2007 - XIV International Symposium on Electromagnetic Fields
in Mechatronics, Electrical and Electronic Engineering
Arras, France, September 10-12, 2009

PERMEANCE COMPUTATION FOR DETERMINATION OF INDUCTION MOTOR ACOUSTIC NOISE

J. Le Besnerais[(1)], V. Lanfranchi[(2)], M. Hecquet[(3)], G. Friedrich[(2)]

(1) ALSTOM TRANSPORT, Valenciennes, France, jean.le-besnerais@transport.alstom.com
(2) LEC- UTC, Centre de recherche de Royallieu, France, vincent.lanfranchi@utc.fr
(3) L2EP- Ecole centrale de Lille, Villeneuve d'Ascq, France, michel.hecquet@ec-lille.fr

Abstract* – The Maxwell pressure is the cause of stator deflection at the origin of acoustic noise radiated by stator. That is why precise determination of air-gap radial flux density B_g is of prime importance. It could be obtained by finite element method, semi numerical or totally analytic method with computation of magneto motive force and permeance. Slot numbers, eccentricity and saturation affecting acoustic behavior can be included in permeance computation with analytic method.

Introduction

Acoustic comfort is an increasingly important factor at the design stage of electric motors [1-3]. Many studies were realized in the past [4,5] and these recent years on several motor types, especially: Switched Reluctance Motor [6,7] and Induction Motor [8-11]. The acoustic noise generated by electric motors can come from aerodynamic noise (fans, windage noise, …), mechanical noise (bearings, …) and magnetic noise which is caused by magnetic forces acting on the active materials of the machine. In some cases (generally: starting phases), the global sound power level (SPL) is dominated by the magnetic noise radiated by the motor and this noise can be quickly annoying as its spectrum contains high tonalities. This study focus on Induction Motor usually chosen for low cost and high reliability quelities, as example, it is the more used traction motor in railway domain.
The Maxwell pressure expressed equation (1) is the cause of stator deflection at the origin of acoustic noise radiated by stator. That is why precise determination of air-gap radial flux density B_g is of prime importance. It could be obtained by numerical method like Finite Element Method (FEM), semi numerical method with help of permeance network or totally analytic method with analytic computation of magneto motive force and permeance. The analytic computation of air-gap permeance is detailed in this article. It is shown that rotor and stator slot numbers, eccentricity and saturation effect can be included in permeance computation to take into account their influence on acoustic behavior. Then, a mechanical and acoustic model of electric motor is quickly described and finally experimental results using these analytic models are shown.

$$P_M = B_g(t,\alpha_s)^2/(2\mu_0) \qquad (1)$$

Flux density computation

Finite Element Method (FEM) is the best method to compute precisely mechanical behavior of machine and electromagnetic forces taking into account saturation, but it is also the most time consuming [12]. Semi numerical methods, with help of permeance network, have almost the same advantages and drawbacks for flux density computation [13-15]. However, a small network does not allow local saturation computation and a big one become time consuming too. Furthermore, permeance network is not useful for geometry modifications. If local saturation is not a main problem, analytic method is suitable to compute electromagnetic forces depending on flux density. This method is the less time consuming and can be precise enough for prediction of acoustic noise tendencies even with saturation effect. The air-gap radial flux density B_g computation is a function of air-gap permeance per unit area and magneto motive force from stator and rotor as shown equation (2). Λ is the permeance per unit area, given by (3), where μ_0 is the air magnetic permeability and g_f is the mean flux density line length of the non constant air-gap taking into account rotor and stator slotting.

$$B_g(t,\alpha_s) = \Lambda(t,\alpha_s)(f_{mm}^s(t,\alpha_s) + f_{mm}^r(t,\alpha_s)) \tag{2}$$

$$\Lambda(t,\alpha_s) = \frac{\mu_0}{g_f(t,\alpha_s)} \tag{3}$$

Computation of airgap permeance including slot numbers, eccentricity and saturation

Slotting effect

As shown equation (3), g_f is the mean flux density line length, approximated as a piecewise constant function which takes four different values (g, g+p_s, g+p_r, g+p_r+p_s) according to the rotor and stator slot relative position [16]. By this way, the permeance function includes slotting effect especially important for spatial order and frequency of excitation forces acting on stator. Table 1 presents some slotting forces expressions with f_s the supply frequency, s the rotor slip, p the number of pole pairs, Z_r and Z_s the numbers of rotor and stator slots and k_r, k_s the harmonic factors. Fig. 1 shows computed evolution (different scales) of permeance, MMF and Maxwell pressure in the airgap.

Table. 1. Spatial order and frequency of main slotting forces expressions

	Frequency f	Spatial order m
F_{slot}^-	$f_s(k_r Z_r(1-s)/p-2)$	$k_r Z_r - k_s Z_s - 2p$
F_{slot}^0	$f_s(k_r Z_r(1-s)/p)$	$k_r Z_r - k_s Z_s$
F_{slot}^+	$f_s(k_r Z_r(1-s)/p+2)$	$k_r Z_r - k_s Z_s + 2p$

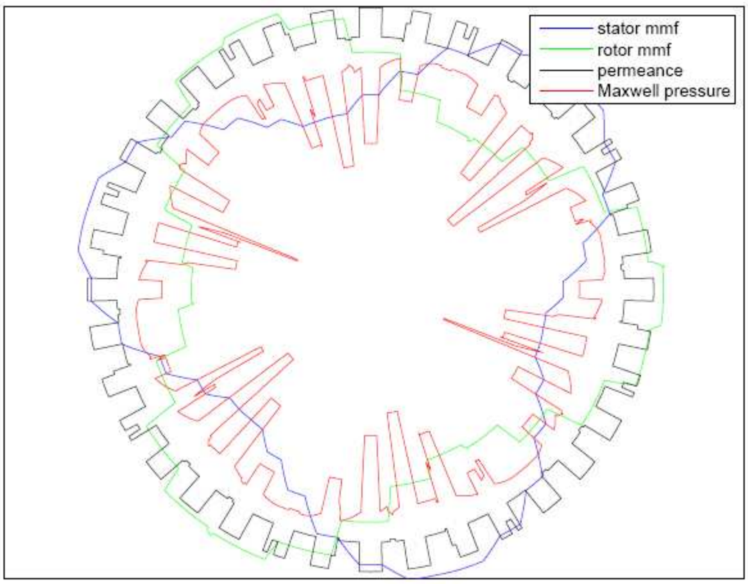

Fig. 1. Airgap Maxwell pressure generated by MMF and permeance.

Eccentricity effect

The rotor eccentricity is the origin of vibrations coming from permeance variations [17,18]. The air-gap is modified: the mean flux density line length (g_f) is function of rotor position as shown Fig. 2. Expressions of fictitious airgap g_f with static (eq. 4) and dynamic (eq 5) eccentricity are given with help of fictitious slot depth (d^f), slot opening location functions (C) and eccentricity factor (λ).

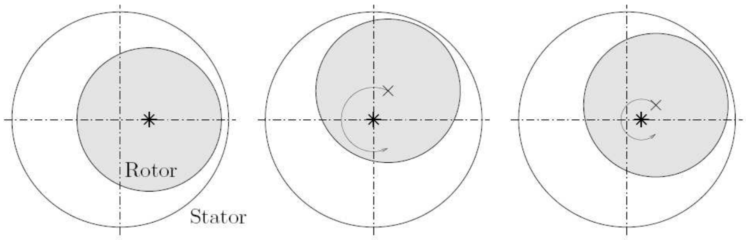

Fig. 2. From left to right : static, dynamic and mixed eccentricity

$$g_f(t,\alpha_s) = (g + d_s^f C_s(\alpha_s) + d_r^f C_r(t,\alpha_s)).(1 - \lambda_{se} cos(\alpha_s)) \quad (4)$$

$$g_f(t,\alpha_s) = (g + d_s^f C_s(\alpha_s) + d_r^f C_r(t,\alpha_s)).(1 - \lambda_{de} cos(\alpha_s - \Omega_r t)) \quad (5)$$

Saturation effect

The permeance is modified in saturated case to account for the flattening of the air-gap flux density [10], as shown Fig. 3 with main saturation harmonics of Table 2, which modifies the magnetic forces spectrum. Saturation phenomenon can actually strongly influence the magnetic noise level.

Table. 2. Spatial order and frequency of main saturation forces expressions

	Frequency f	Spatial order m
F_{sat}^-	$f_s(k_r Z_r(1-s)/p - 2(1+k_a))$	$k_r Z_r - k_s Z_s - 2p(1+k_a)$
F_{sat}^0	$f_s(k_r Z_r(1-s)/p \pm 2k_a)$	$k_r Z_r - k_s Z_s \pm 2pk_a$
F_{sat}^+	$f_s(k_r Z_r(1-s)/p + 2(1+k_a))$	$k_r Z_r - k_s Z_s + 2p(1+k_a)$

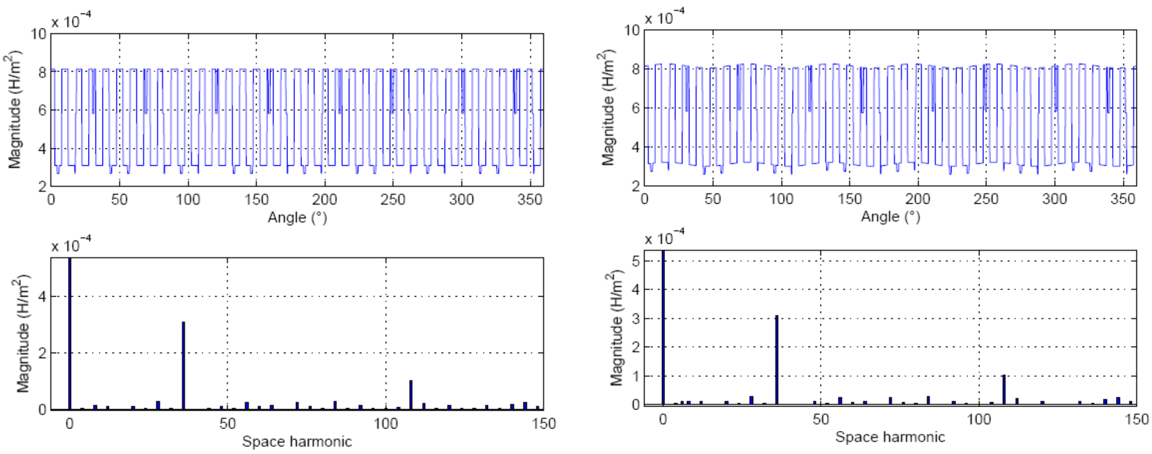

Fig. 3. Waveform and spectra of permeance, left : without saturation, right : with saturation.

Exciting force and mechanical model

Mechanical model

The force distribution (Maxwell pressure) is developed into a 2D Fourier series of force waves P_{mw} with spatial frequencies (spatial order) m and frequency f (Fig. 4).

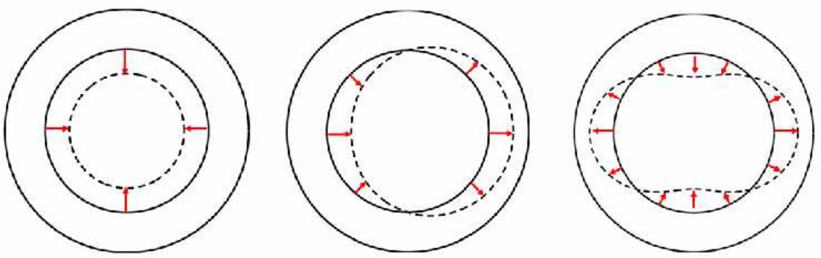

Fig. 4. Illustration of the pressure distribution decomposition in sinusoidal force waves of order 0, 1 and 2.

The stator is then modeled as a 2D ring, and its static deflections under the sinusoidal loads P_{mw} can be analytically computed. For instance, for m>1

$$Y_{mw}^{s} = 12 R_a R_m{}^3 P_{mw} / (E h^3 (m^2 - 1)^2) \tag{6}$$

where h is the thickness of the stator back core (yoke), R_m is the mean stator radius (computed without considering the teeth), E is the stator's Young modulus in radial direction and R_a is the stator bore radius. Then, dynamic displacements Y^d_{mw} are computed through a second order transfer function:

$$Y_{mw}^{d} = Y_{mw}^{s} \left[(1 - f^2 / f_m{}^2)^2 + 4 \zeta_m{}^2 f^2 / f_m{}^2 \right]^{-1/2} \tag{7}$$

where ξ_m is the damping coefficient, and f_m is the m-th stator circumferential mode natural frequency. ξ_m lie between 1% and 4%, it is computed using the experimental established by Yang [3]. The natural frequencies are computed modeling the stator sheet as a 2D ring. For m $\geq$ 2 they are expressed as [1]:

$$f_m = f_0 h\, m (m^2 - 1) / (2\sqrt{3} R_m \sqrt{m^2 + 1}) \qquad f_0 = \sqrt{E / (\Delta \rho)} / (2 \pi R_m) \tag{8}$$

where f_0 is the zero mode natural frequency, ρ is the stator mass per unit volume, and Δ is the stator mass corrective factor which includes the effect of windings and teeth mass. The natural frequencies computation was validated by FEM and tests [10,11], with some operational or experimental modal analysis.

Acoustic model

The velocity vibration waves v_{mw} and the associated radiated power W_m are then computed as

$$v_{mw} = \omega Y_{mw}^{d} \qquad W_m(f) = \rho_0 c S \sigma_m(f) \left| v_{mw} \right|^2 / 2 \tag{9}$$

where σ_m is the radiation factor, ρ_0 the air density, c the speed of sound and S the stator outer surface including frame. The radiation factor computation is analytically computed using the model of a pulsating sphere [2]. The total sound power $W(f)$ is the sum of the sound power radiated by each mode. The total sound power level associated to a given frequency is then :

$$L_w(f) = 10\log_{10}(W(f)/W_0), \quad W_0 = 10^{-12}\,W \tag{10}$$

Experimental results

Figure 5 presents an experimental sonogram of a 250 kW traction motor in adjustable speed drive. This sonogram shows evolution of spectra with time (knowing that motor speed is varying with time thanks to supply frequency from 0 to 200 Hz). Frequency range is limited to the area of maximum noise (0 to 3.2 kHz). One can see around 800 Hz the major source of noise caused by saturation as predicted by analytic model (Fig. 6).

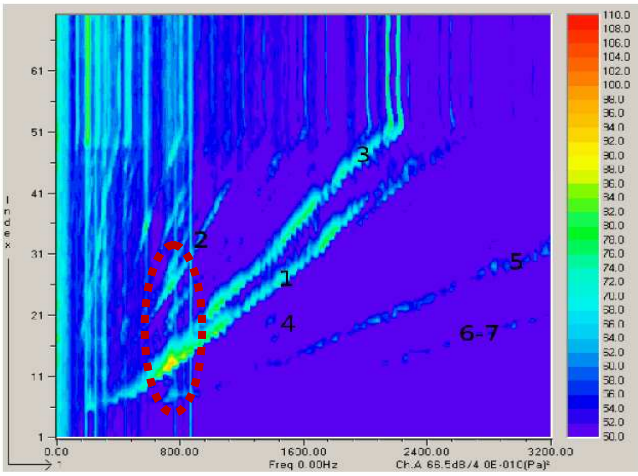

Fig. 5. Measured sonogram of a water-cooled 250 kW traction motor in sinusoidal off-load case (f_s=0 to 200 Hz).

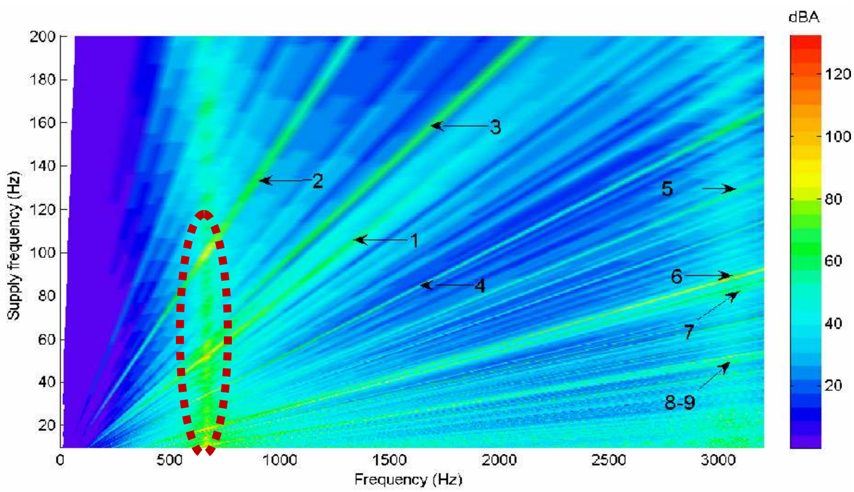

Fig. 6. Simulated sonogram of a 250 kW traction motor in sinusoidal off-load case (f_s=0 to 200 Hz).

Conclusion

The Maxwell pressure is the cause of stator deflection at the origin of acoustic noise radiated by stator. That is why precise determination of air-gap radial flux density B_g is of prime importance. Analytic computation of magneto motive force and permeance gives flux density. This article shows that slot numbers, eccentricity and saturation effect can be efficiently included in permeance computation. Simulated acoustic results using electromagnetic and mechanical analytic models show good accuracy with experimental results. This method is now used to improve acoustic behavior of induction motors at design stage.

References

[1] J.F. Gieras, C. Wang and J.C. Lai, Noise of polyphase electric motors, CRC Press, 2005.

[2] P.L. Timar, Noise and vibration of electrical machines, Elsevier, 1989.

[3] S.J. Yang, Low noise electrical motors, Clarendon Press, Oxford, 1981.

[4] H. Jordan, Electric motor silencer - formation and elimination of the noises in the electric motors, W. Giradet-Essen editor, 1950.

[5] P. Alger, The Nature of Polyphase Induction Machines, John Wiley & Sons, Inc., 1951.

[6] J. P. Lecointe, R. Romary, J. F. Brudny, M. McClelland, Analysis and active reduction of vibration and acoustic switched reluctance motor. Electric Power Applications, IEE, Vol 51, pp 725-733, 2004.

[7] X. Mininger, Réduction des vibrations des machines à réluctance variable à l'aide d'actionneurs piézoélectriques, PhD thesis, ENS Cachan, 2005.

[8] B. Cassoret, R. Corton, D. Roger, J. Brudny, Magnetic noise reduction of induction machines, IEEE Trans. on Power Electronics, Vol 18, N°2, pp 570-579, 2003.

[9] V. Lanfranchi, G. Friedrich, J. Le Besnerais, M. Hecquet, Spread spectrum strategies study for induction motor vibratory and acoustic behavior, IEEE IECON 2006, Paris, 2006.

[10] J. Le Besnerais, V. Lanfranchi, M. Hecquet and P. Brochet, Characterisation and reduction of magnetic noise due to saturation in induction machines, IEEE Trans. on Mag. Vol 45, N°4 pp 2003-2008, april 2009.

[11] J. Le Besnerais, V. Lanfranchi, M. Hecquet, P. Brochet, and G. Friedrich, Acoustic noise of electromagnetic origin in a fractional-slot induction machine, COMPEL, Vol 27, N°5, pp 1033-1052, 2008.

[12] M. E. H. Benbouzid, G. Reyne, S. Derou, and A. Foggia, Finite element modeling of a synchronous machines: electromagnetic forces and mode shapes, IEEE Trans. On Mag., Vol. 29, pp. 2014–2018, 1993.

[13] Petrichenko, D. Contribution à la modelisation et la conception optimale des turbo-alternateurs. PhD thesis, Ecole Centrale de Lille, France, 2006.

[14] Augustin Delale, Laurent Albert, Laurent Gerbaud, and Frédéric Wurtz, Automatic Generation of Sizing Models for the Optimization of Electromagnetic Devices Using Reluctance Networks, IEEE Trans. On Mag, Vol. 40, N°. 2, pp830 – 833, March 2004,.

[15] S. Srairi, J. Farook, A. Djerdir, A. Miraoui, The magnetic network modeling of a permanent magnet motor with consideration of the saturation and heating effects, ISEF'2005, Spain, Sept. 2005.

[16] J. F. Brudny, Modélisation de la denture des machines asynchrones : phénomènes de résonances, J. Phys. III, Vol 7, pp 1009-1023, 1997.

[17] S. Ayari, Etude des vibrations des machines à reluctance variable: influence des caractéristiques géométriques et de l'excentricité rotorique, PhD Thesis, ENS Cachan, 2000.

[18] M. Blodt, J. Regnier, J. Faucher, Distinguishing Load Torque Oscillations and Eccentricity Faults in Induction Motors Using Stator Current Wigner Distribution, in Proc. IEEE Industry Applications Society Annual Meeting 2006, Tampa, Florida, Oct. 2006.